A decoupling algorithm for fluid-structure interaction problems based on optimization

Paul Kuberry * Hyesuk Lee †

Abstract

Simulating fluid-structure interactions is challenging due to the tight coupling between the fluid and solid substructures. Explicit and implicit decoupling methods often either fail or require relaxation when densities of the two materials are close. In this paper, a fluid-structure interaction problem is formulated as a least squares problem, where the jump in velocities of the two substructures is minimized by a Neumann control enforcing the continuity of stress on the interface. A decoupling optimization algorithm is discussed, which requires few nonlinear solves at each time step, and numerical results are presented.

Key words optimal control, fluid-structure interaction, finite element method

1 Introduction

Modelling fluid-structure interaction (FSI) problems is of great practical importance for applications ranging from blood flow to micromixing [4, 5, 7, 9, 16, 24, 19, 22, 23]. There are a wide variety of methods for simulating the coupled FSI system, but each is limited by factors including computational complexity and stability. Possibilities include a monolithic formulation of the problem, which is computationally complex due to requiring many large matrix solves to converge on a solution to the nonlinear system. Additional difficulties with this method include the development of efficient and appropriate preconditioners for the matrix resulting from the discretized system.

A common approach is decoupling the fluid and structure subsystems, permitting use of partitioned solvers which may be more attractive and allow the use of legacy codes. This also allows for operations on a smaller matrix for each subsystem solve. For a partitioned method, difficulties arise in how to iterate between the two subsystems. Implicit and explicit possibilities exist; implicit iterations generally requiring many nonlinear subsystem solves and explicit iterations requiring fewer nonlinear subsystem solves, but with a degradation in stability. When the magnitude of the densities of the structure and fluid are close, decoupling methods using explicit iterations tend to fail and even implicit iterations

*Department of Mathematical Sciences, Clemson University, Clemson, SC 29630 (pkuberr@clemson.edu), Partially supported by the NSF under grant no. DMS-1016182.

†Department of Mathematical Sciences, Clemson University, Clemson, SC 29634 (hklee@clemson.edu), Partially supported by the NSF under grant no. DMS-1016182.

become unstable. Introduction of pressure penalization [6] or relaxation in updating subsystem solutions [8, 17] may be introduced to increase stability. Relaxation schemes are less successful the closer the two densities are in magnitude, and often they increase the computational complexity by introducing many more nonlinear subsystem solves. For areas such as aerospace engineering, the large difference in densities of the subsystems permits more efficient simulation. However, for blood flow modelling, often the density of the vessel and fluid are nearly identical.

Murea and Sy [18] have studied an algorithm for FSI, based on optimization, using both a linear and nonlinear elastic formulation for the structure. In their approach for the linear formulation, they expand a function along the interface by its eigenfunctions and solve for coefficients to the inner product by use of optimization. This allows them to optimize a smaller number of unknowns. They use the stress on the interface as a Neumann control for solving the structure subsystem. Then, enforcing continuity of velocity through a Dirichlet boundary condition for the fluid subsystem, they update the control and repeat the process until the stress discontinuity on the interface is sufficiently small. This process requires that the subsystem solves must be made in serial.

An alternative approach we present here is inspired by domain decomposition methods that have been explored by Gunzburger and Lee in [15] for solving the Navier-Stokes equations. In the approach, the computational domain is split into two subdomains using an artificial interface and a subproblem of the same governing equations is solved on each subdomain. The stress between the two subsystems is prescribed and updated through Gauss-Newton iterations so that it minimizes the discontinuity of the fluid velocity on the artificial interface. Similarly, in [11], this idea was used for the Stokes-Darcy equations. Because the stress is prescribed for the fluid and structure subsystem as a Neumann boundary condition, both nonlinear subsystem solves may be made in parallel.

This paper is organized as follows. In the next section, we describe model equations, the variational formulation based on the Arbitrary Lagrangian Eulerian (ALE) method, and time discretizations. With a desire to decouple the monolithic formulation of the FSI problem, we introduce, in Section 3, an implicit iteration method that finds the stress on the interface at each time step which minimizes the jump between the fluid and structure velocities. It is similar to [11], however the interface is now natural and is determined by where the fluid and structure subproblems meet. Our optimization technique uses Gauss-Newton iterations to update the interface as well as the stress on the interface, generally requiring only 2 or 3 nonlinear subsystem solves per time step. How to compute updates to the stress on the interface requires solving a linear least squares problem, which can be handled by iterative solver of choice. Section 4 presents numerical results and method comparisons, and conclusion follows in Section 5.

2 ALE formulation and time discretization for model equations

The fluid-structure interaction we will consider is an incompressible Newtonian fluid and an isotropic linear elastic structure.

Let Ω_t^f be a bounded moving fluid domain at time t in $\mathbb{R}^2$ with the boundary Γ_t^f such

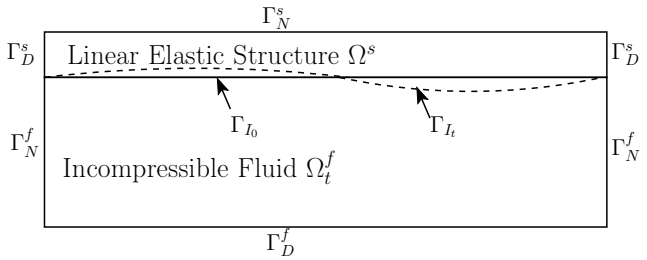

Figure 1: Fluid-Structure Interaction Domain

that $\Gamma_t^f = \Gamma_N^f \cup \Gamma_D^f \cup \Gamma_{I_t}$, where Γ_{I_t} is a moving boundary. Also let Ω^s be a fixed structure domain with the boundary Γ^s such that $\Gamma^s = \Gamma_N^s \cup \Gamma_D^s \cup \Gamma_{I_0}$, where Γ_{I_0} is the movable fluid boundary at time 0. Consider the system of fluid and structure equations

$$\rho_f \left(\frac{\partial \mathbf{u}}{\partial t} + \mathbf{u} \cdot \nabla \mathbf{u} \right) - 2\nu_f \nabla \cdot D(\mathbf{u}) + \nabla p = \mathbf{f}_f \quad \text{in } \Omega_t^f , \tag{2.1}$$

$$\nabla \cdot \mathbf{u} = 0 \quad \text{in } \Omega_t^f , \tag{2.2}$$

$$\rho_s \frac{\partial^2 \boldsymbol{\eta}}{\partial t^2} - 2\nu_s \nabla \cdot D(\boldsymbol{\eta}) - \lambda \nabla \cdot (\nabla \cdot \boldsymbol{\eta}) = \mathbf{f}_s \quad \text{in } \Omega^s , \tag{2.3}$$

where $\mathbf{u}$ denotes the velocity vector of fluid, p the pressure of fluid, ρ_f the density of the fluid, ν_f the fluid viscosity, $\boldsymbol{\eta}$ the displacement of structure, and ρ_s the structure density. In (2.1) and (2.3), $D(\cdot)$ is the rate of the strain tensor, i.e., $D(\mathbf{v}) := (\nabla \mathbf{v} + \nabla \mathbf{v}^T)/2$. The Lam*é* parameters are denoted by ν_s and λ, and the body forces are denoted by $\mathbf{f}_f$ and $\mathbf{f}_s$. Initial and boundary conditions for $\mathbf{u}$ and $\boldsymbol{\eta}$ are given as follows:

$$2\nu_f D(\mathbf{u})\mathbf{n}_f - p\mathbf{n}_f = \mathbf{u}_N \quad \text{on } \Gamma_N^f , \tag{2.4}$$

$$\mathbf{u} = \mathbf{0} \quad \text{on } \Gamma_D^f , \tag{2.5}$$

$$2\nu_s D(\boldsymbol{\eta})\mathbf{n}_s + \lambda(\nabla \cdot \boldsymbol{\eta})\mathbf{n}_s = \boldsymbol{\eta}_N \quad \text{on } \Gamma_N^s , \tag{2.6}$$

$$\boldsymbol{\eta} = \mathbf{0} \quad \text{on } \Gamma_D^s , \tag{2.7}$$

$$\mathbf{u}(\mathbf{x}, 0) = \mathbf{u}^0 \quad \text{in } \Omega_0^f , \tag{2.8}$$

$$\boldsymbol{\eta}(\mathbf{x}, 0) = \boldsymbol{\eta}^0 \quad \text{in } \Omega^s , \tag{2.9}$$

$$\boldsymbol{\eta}_t(\mathbf{x}, 0) = \dot{\boldsymbol{\eta}}^0 \quad \text{in } \Omega^s , \tag{2.10}$$

where $\dot{\boldsymbol{\eta}}^0 = \mathbf{u}_0$. The moving boundary Γ_{I_t} is determined by the displacement $\boldsymbol{\eta}$ at time t (Fig. 1). The interface conditions between the fluid and the structure are obtained by enforcing continuity of the velocity and the stress force:

$$\frac{\partial \boldsymbol{\eta}}{\partial t} = \mathbf{u} \quad \text{on } \Gamma_{I_t} , \tag{2.11}$$

$$2\nu_f D(\mathbf{u})\mathbf{n}_f - p\mathbf{n}_f = -(2\nu_s D(\boldsymbol{\eta})\mathbf{n}_s + \lambda(\nabla \cdot \boldsymbol{\eta})\mathbf{n}_s) \quad \text{on } \Gamma_{I_t} . \tag{2.12}$$

The Arbitrary Lagrangian Eulerian (ALE) [10] method is one of the most widely used numerical schemes in simulating fluid flows in a moving domain. In the ALE formulation, a one-to-one coordinate transformation is introduced for the fluid domain, and the fluid equations can be rewritten with respect to a fixed reference domain. Specifically, we define the time-dependent bijective mapping Ψ_t which maps the reference domain Ω_0 to the physical domain Ω_t:

$$\Psi_t : \Omega_0 \to \Omega_t, \qquad \Psi_t(\mathbf{y}) = \mathbf{x}(\mathbf{y}, t)\,, \tag{2.13}$$

where $\mathbf{y}$ and $\mathbf{x}$ are the spatial coordinates in Ω_0 and Ω_t, respectively. The coordinate $\mathbf{y}$ is often called the *ALE coordinate*. Using Ψ_t, the weak formulation of the flow equations in Ω_t can be recast into a weak formulation defined in the reference domain Ω_0. Thus, the model equations in the reference domain can be considered for numerical simulation and the transformation function Ψ_t needs to be determined at each time step as a part of computation.

For a function $\phi : \Omega_t \times [0, T] \to \mathbb{R}$, its corresponding function $\overline{\phi} = \phi \circ \Psi_t$ in the ALE setting is defined as

$$\overline{\phi} : \Omega_0 \to \mathbb{R}, \qquad \overline{\phi}(\mathbf{y}, t) = \phi(\Psi_t(\mathbf{y}), t). \tag{2.14}$$

The time derivative in the ALE frame is also given as

$$\frac{\partial \phi}{\partial t}\,|_{\mathbf{y}} \colon \Omega_t \times [0, T] \to \mathbb{R}\,, \qquad \frac{\partial \phi}{\partial t}\,|_{\mathbf{y}}\,(\mathbf{x}, t) = \frac{\partial \overline{\phi}}{\partial t}(\mathbf{y}, t). \tag{2.15}$$

Using the chain rule, we have

$$\frac{\partial \phi}{\partial t}\,|_{\mathbf{y}} = \frac{\partial \phi}{\partial t}\,|_{\mathbf{x}} + \mathbf{z} \cdot \nabla_{\mathbf{x}} \phi, \tag{2.16}$$

where $\mathbf{z} := \frac{\partial \mathbf{x}}{\partial t}\,|_{\mathbf{y}}$ is the domain velocity. In (2.16) $\frac{\partial \phi}{\partial t}\,|_{\mathbf{y}}$ is the so-called *ALE derivative* of ϕ. The flow equations (2.1)-(2.2) can then be written in ALE formulation as

$$\rho_f \left(\frac{\partial \mathbf{u}}{\partial t}\,|_{\mathbf{y}} + (\mathbf{u} - \mathbf{z}) \cdot \nabla_{\mathbf{x}} \mathbf{u} \right) - 2\nu_f \nabla_{\mathbf{x}} \cdot D_{\mathbf{x}}(\mathbf{u}) + \nabla_{\mathbf{x}} p = \mathbf{f}_f \quad \text{in } \Omega_t^f\,, \tag{2.17}$$

$$\nabla_{\mathbf{x}} \cdot \mathbf{u} = 0 \quad \text{in } \Omega_t^f\,, \tag{2.18}$$

where $D_{\mathbf{x}}(\mathbf{u}) = (\nabla_{\mathbf{x}} \mathbf{u} + \nabla_{\mathbf{x}} \mathbf{u}^T)/2$. Note that all spatial derivatives involved in (2.17)-(2.18), including the divergence operator, are with respect to $\mathbf{x}$. Throughout the paper we will use $D_{\mathbf{x}}(\cdot)$ and $\nabla_{\mathbf{x}}$ only when they need to be clearly specified. Otherwise, $D(\cdot)$, ∇ will be used as $D_{\mathbf{x}}(\cdot)$, $\nabla_{\mathbf{x}}$, respectively.

We use the Sobolev spaces $W^{m,p}(D)$ with norms $\|\cdot\|_{m,p,D}$ if $p < \infty$, $\|\cdot\|_{m,\infty,D}$ if $p = \infty$. Denote the Sobolev space $W^{m,2}$ by H^m with the norm $\|\cdot\|_{m,D}$. The corresponding space of vector-valued or tensor-valued functions is denoted by $\mathbf{H}^m$.

For the variational formulation of the flow equations (2.17)-(2.18) in the ALE framework, define function spaces for the reference domain:

$$U_0 := \{\mathbf{v} \in \mathbf{H}^1(\Omega_0^f) : \mathbf{v} = \mathbf{0} \text{ on } \Gamma_D^f\}\,,$$
$$Q_0 := L^2(\Omega_0^f)\,.$$

The function spaces for Ω_t are then defined as

$$\mathbf{U}_t := \{\mathbf{v} : \Omega_t \times [0,T] \to \mathbb{R}^2,\ \mathbf{v} = \overline{\mathbf{v}} \circ \Psi_t^{-1} \text{ for } \overline{\mathbf{v}} \in \mathbf{U}_0\},$$
$$Q_t := \{q : \Omega_t \times [0,T] \to \mathbb{R},\ q = \overline{q} \circ \Psi_t^{-1} \text{ for } \overline{p} \in Q_0\}.$$

The variational formulation for $(\mathbf{u}, p)$ in ALE framework is given by: find $(\mathbf{u}, p)$ such that

$$\rho_f \left(\frac{\partial \mathbf{u}}{\partial t} \mid_{\mathbf{y}} + (\mathbf{u} - \mathbf{z}) \cdot \nabla \mathbf{u},\ \mathbf{v} \right)_{\Omega_t} + 2\nu_f (D(\mathbf{u}), D(\mathbf{v}))_{\Omega_t} - (p, \nabla \cdot \mathbf{v})_{\Omega_t}$$
$$= (\mathbf{f}_f, \mathbf{v})_{\Omega_t} + (\mathbf{u}_N, \mathbf{v})_{\Gamma_N^f} + (\mathbf{g}, \mathbf{v})_{\Gamma_{I_t}} \ \forall \mathbf{v} \in \mathbf{U}_t, \tag{2.19}$$

$$(q, \nabla \cdot \mathbf{u})_{\Omega_t} = 0 \quad \forall q \in Q_t, \tag{2.20}$$

where we set $\mathbf{g} := 2\nu_f D(\mathbf{u})\mathbf{n}_f - p\mathbf{n}_f \mid_{\Gamma_{I_t}}$.

For the structure displacement $\boldsymbol{\eta}$ and velocity $\dot{\boldsymbol{\eta}}$, define the function space

$$\boldsymbol{\Sigma} := \{\boldsymbol{\xi} \in \mathbf{H}^1(\Omega^s) : \boldsymbol{\xi} = \mathbf{0} \text{ on } \Gamma_D^s\},$$

and consider the variational formulation:

$$\rho_s \left(\frac{\partial^2 \boldsymbol{\eta}}{\partial t^2}, \boldsymbol{\xi} \right)_{\Omega^s} + 2\nu_s (D(\boldsymbol{\eta}), D(\boldsymbol{\xi}))_{\Omega^s} + \lambda (\nabla \cdot \boldsymbol{\eta}, \nabla \cdot \boldsymbol{\xi})_{\Omega^s}$$
$$= (\mathbf{f}_s, \boldsymbol{\xi})_{\Omega^s} + (\boldsymbol{\eta}_N, \boldsymbol{\xi})_{\Gamma_N^s} - (\mathbf{g}, \boldsymbol{\xi} \circ \Psi_t^{-1})_{\Gamma_{I_t}} \ \forall \boldsymbol{\xi} \in \boldsymbol{\Sigma}, \tag{2.21}$$

where the interface condition (2.12) has been imposed though the function $\mathbf{g}$.

In order to define the ALE mapping Ψ_t, we consider the boundary position function $h : \Gamma_{I_0} \times [0,T] \to \Gamma_{I_t}$. The ALE mapping may be then determined by solving the Laplace equation

$$\begin{aligned} \Delta_{\mathbf{y}} \mathbf{x}(\mathbf{y}) &= 0 && \text{in } \Omega_0, \\ \mathbf{x}(\mathbf{y}) &= h(\mathbf{y}) && \text{on } \Gamma_{I_0}. \end{aligned} \tag{2.22}$$

This method is called the *harmonic extension technique*, where the boundary position function h is extended onto the whole domain [12].

Consider the time discretized fluid problem by the standard implicit Euler method using the Reynold's Transport formula [20]

$$\frac{d}{dt} \int_{V(t)} \boldsymbol{\phi}(\mathbf{x}, t)\, dV = \int_{V(t)} \frac{\partial \boldsymbol{\phi}}{\partial t} \mid_{\mathbf{y}} + \boldsymbol{\phi} \nabla_{\mathbf{x}} \cdot \mathbf{z}\, dV \tag{2.23}$$

for a function $\boldsymbol{\phi} : V(t) \to \mathbb{R}$, where $V(t) \subset \Omega_t$ such that $V(t) = \Psi_t(V_0)$ with $V_0 \subset \Omega_0$. If $\mathbf{v}$ is a function from Ω_t to $\mathbb{R}$ and $\mathbf{v} = \overline{\mathbf{v}} \circ \Psi_t^{-1}$ for $\mathbf{v} : \Omega_0 \to \mathbb{R}$, we have that $\frac{\partial \mathbf{v}}{\partial t}|_y = 0$ and therefore

$$\frac{d}{dt} \int_{\Omega_t} \boldsymbol{\phi} \mathbf{v}\, d\Omega = \int_{\Omega_t} \left(\frac{\partial \boldsymbol{\phi}}{\partial t} \mid_{\mathbf{y}} + \boldsymbol{\phi} \nabla_{\mathbf{x}} \cdot \mathbf{z} \right) \mathbf{v}\, d\Omega. \tag{2.24}$$

Using (2.24), (2.19)-(2.20) become

$$\rho_f \frac{d}{dt}\left(\mathbf{u},\,\mathbf{v}\right)_{\Omega_t} + \rho_f\left((\mathbf{u}-\mathbf{z})\cdot\nabla\mathbf{u},\,\mathbf{v}\right)_{\Omega_t} - \rho_f(\mathbf{u}(\nabla\cdot\mathbf{z}),\mathbf{v})_{\Omega_t} + 2\nu_f(D(\mathbf{u}),D(\mathbf{v}))_{\Omega_t}$$
$$-(p,\nabla\cdot\mathbf{v})_{\Omega_t} \;=\; (\mathbf{f}_f,\mathbf{v})_{\Omega_t} + (\mathbf{u}_N,\mathbf{v})_{\Gamma_N^f} + (\mathbf{g},\mathbf{v})_{\Gamma_{I_t}} \;\forall\mathbf{v}\in\mathbf{U}_t\,, \tag{2.25}$$

$$(q,\nabla\cdot\mathbf{u})_{\Omega_t} = 0 \quad \forall q\in Q_t\,, \tag{2.26}$$

and temporal discretization by implicit Euler further yields

$$\rho_f\left[(\mathbf{u}^n,\mathbf{v})_{\Omega_{t_n}^f} - (\mathbf{u}^{n-1},\mathbf{v})_{\Omega_{t_{n-1}}^f}\right] + \Delta t\,\rho_f\left[((\mathbf{u}^n-\mathbf{z}^n)\cdot\nabla\mathbf{u}^n,\mathbf{v})_{\Omega_{t_n}^f}\right.$$
$$\left.-(\mathbf{u}^n(\nabla\cdot\mathbf{z}^n),\mathbf{v})_{\Omega_{t_n}^f}\right] + \Delta t\left[2\nu_f(D(\mathbf{u}^n),\,D(\mathbf{v}))_{\Omega_{t_n}^f} - (p^n,\nabla\cdot\mathbf{v})_{\Omega_{t_n}^f}\right]$$
$$= \Delta t\left[(\mathbf{f}_f^n,\mathbf{v})_{\Omega_{t_n}^f} + (\mathbf{u}_N^n,\mathbf{v})_{\Gamma_N^f} + (\mathbf{g}^n,\mathbf{v})_{\Gamma_{I_n}}\right]\;\forall\mathbf{v}\in\mathbf{U}_{t_n}\,, \tag{2.27}$$

$$(q,\nabla\cdot\mathbf{u}^n)_{\Omega_{t_n}^f} = 0 \quad \forall q\in Q_{t_n}\,. \tag{2.28}$$

For optimization problems introduced in the next section, two time discretizations of the structure subsystem will be considered. The first is a first order time discretization of the structure problem given by

$$\rho_s\left(\boldsymbol{\eta}^n - 2\boldsymbol{\eta}^{n-1} + \boldsymbol{\eta}^{n-2},\boldsymbol{\xi}\right)_{\Omega^s} + \Delta t^2\left[2\nu_s\left(D(\boldsymbol{\eta}^n),D(\boldsymbol{\xi})\right)_{\Omega^s} + \lambda\left(\nabla\cdot(\boldsymbol{\eta}^n)\,,\nabla\cdot\boldsymbol{\xi}\right)_{\Omega^s}\right]$$
$$= \Delta t^2\left[(\mathbf{f}_s^n,\boldsymbol{\xi})_{\Omega^s} + (\boldsymbol{\eta}_N^n,\boldsymbol{\xi})_{\Gamma_N^s} - (\mathbf{g}^n,\boldsymbol{\xi}\circ\Psi_n^{-1})_{\Gamma_{I_n}}\right]\;\forall\boldsymbol{\xi}\in\boldsymbol{\Sigma} \tag{2.29}$$

and the next is a second order time discretization of the structure problem given by

$$\rho_s\left(\dot{\boldsymbol{\eta}}^n - \dot{\boldsymbol{\eta}}^{n-1},\boldsymbol{\xi}\right)_{\Omega^s}$$
$$+\Delta t\left[2\,\nu_s\left(\frac{D(\boldsymbol{\eta}^n)+D(\boldsymbol{\eta}^{n-1})}{2},D(\boldsymbol{\xi})\right)_{\Omega^s} + \lambda\left(\nabla\cdot\left(\frac{\boldsymbol{\eta}^n+\boldsymbol{\eta}^{n-1}}{2}\right),\nabla\cdot\boldsymbol{\xi}\right)_{\Omega^s}\right]$$
$$= \Delta t\left[\left(\frac{\mathbf{f}_s^n+\mathbf{f}_s^{n-1}}{2},\boldsymbol{\xi}\right)_{\Omega^s} + \left(\frac{\boldsymbol{\eta}_N^n+\boldsymbol{\eta}_N^{n-1}}{2},\boldsymbol{\xi}\right)_{\Gamma_N^s} - (\mathbf{g}^n,\boldsymbol{\xi}\circ\Psi_n^{-1})_{\Gamma_{I_n}}\right]$$
$$\forall\boldsymbol{\xi}\in\boldsymbol{\Sigma}\,, \tag{2.30}$$

$$\left(\boldsymbol{\eta}^n - \boldsymbol{\eta}^{n-1},\boldsymbol{\gamma}\right)_{\Omega^s} - \Delta t\left(\frac{\dot{\boldsymbol{\eta}}^n+\dot{\boldsymbol{\eta}}^{n-1}}{2},\boldsymbol{\gamma}\right)_{\Omega^s} = 0\;\forall\boldsymbol{\gamma}\in\boldsymbol{\Sigma}\,. \tag{2.31}$$

3 Domain decomposition by optimization

It is desirable that an algorithm for solving FSI problems be able to stably decouple the subsystems and solve each subsystem in parallel. Stably decoupling the subsystems is of particular importance in the case when the added mass effect is present.

We will now consider solving our FSI problem in the context of an optimal control problem, which allows us to enforce a common stress on the interface at every iteration of

optimization. Few nonlinear iterations are needed to solve the FSI problem at each time step via Gauss-Newtons iterations used to compute the optimal stress that minimizes the jump in velocities across the moving interface. This approach does not require relaxation, such as would be needed for a Dirichlet-Neumann decoupling[7] due to a stability issue.

An additional feature of this algorithm is that it allows for parallel solving of the nonlinear fluid and structure problems, as well as parallel solving of the adjoint and linearized subproblems in each Gauss-Newton iteration. This computational cost savings would be even more significant if applied to an FSI problem with a nonlinear structure model.

Let us begin by letting the stress function $\mathbf{g}^n$ in (2.27) and (2.29) or (2.30) be chosen as a control in each time step to enforce the continuity of velocity (2.11), i.e., we wish to minimize the penalized functional

$$\mathcal{J}_n(\mathbf{u}^n, \dot{\boldsymbol{\eta}}^n, \mathbf{g}^n) = \frac{1}{2}\int_{\Gamma_{I_n}} |\mathbf{u}^n - \dot{\boldsymbol{\eta}}^n \circ \Psi_n^{-1}|^2 \, d\Gamma + \frac{\epsilon}{2}\int_{\Gamma_{I_n}} |\mathbf{g}^n|^2 \, d\Gamma \,, \tag{3.1}$$

subject to (2.27)-(2.28) and (2.29) or (2.27)-(2.28) and (2.30)-(2.31), depending on the structure formulation used. If using the first order discretization of the structure subsystem (2.29), $\dot{\boldsymbol{\eta}}^n$ in (3.1) can be approximated by

$$\dot{\boldsymbol{\eta}}^n \approx \frac{\boldsymbol{\eta}^n - \boldsymbol{\eta}^{n-1}}{\Delta t}.$$

In (3.1), ϵ is the penalty parameter which gives relative weight to the latter term and Γ_{I_n} denotes the interface at time step n, to be determined by the solution to (2.29) or (2.27)-(2.28) using Gauss-Newton iterations described later in Algorithm 3.3. Our approach is an implicit algorithm for the fluid-structure interaction problem.

We use nonlinear least squares to develop a computational algorithm for the constrained optimal control problem.

Define the nonlinear operator $N_n : \mathbf{L}^2(\Gamma_{I_n}) \to \mathbf{L}^2(\Gamma_{I_n}) \times \mathbf{L}^2(\Gamma_{I_n})$ by

$$N_n(\mathbf{g}^n) = \begin{pmatrix} (\mathbf{u}^n - \dot{\boldsymbol{\eta}}^n \circ \Psi_n^{-1}) \mid_{\Gamma_{I_n}} \\ \sqrt{\epsilon}\, \mathbf{g}^n \end{pmatrix},$$

where $\mathbf{u}^n$, $\dot{\boldsymbol{\eta}}^n$ are the fluid and structure velocities satisfying (2.27)-(2.31) when $\mathbf{g}^n$ is the stress function on the interface. Then, (3.1) can be written as

$$\mathcal{J}_n(\mathbf{g}^n) = \frac{1}{2}\|N_n(\mathbf{g}^n)\|^2_{\mathbf{L}^2(\Gamma_{I_n})\times\mathbf{L}^2(\Gamma_{I_n})} \tag{3.2}$$

and the nonlinear least squares problem we consider is to

$$\textit{seek } \mathbf{g}^n \in \mathbf{L}^2(\Gamma_{I_n}) \textit{ such that } (3.2) \textit{ is minimized.} \tag{3.3}$$

We can linearize $N_n(\mathbf{g}^n)$ using the Fréchet derivative of $N_n(\cdot)$ at $\overline{\mathbf{g}}^n$, $N_n'(\overline{\mathbf{g}}^n)$, by

$$N_n(\mathbf{g}) = N_n(\overline{\mathbf{g}}^n) + N'(\overline{\mathbf{g}}_n)(\mathbf{g}^n - \overline{\mathbf{g}}^n) + O(\|\mathbf{g}^n - \overline{\mathbf{g}}^n\|^2_{\mathbf{L}^2(\Gamma_{I_n})\times\mathbf{L}^2(\Gamma_{I_n})})$$

so that solutions of the nonlinear least squares problem can be obtained by repeatedly solving the linear least squares problem

$$\min_{\mathbf{h}^n \in \mathbf{L}^2(\Gamma_{I_n})} \frac{1}{2}\|N(\overline{\mathbf{g}}^n) + N_n'(\overline{\mathbf{g}}^n)\mathbf{h}^n\|^2_{\mathbf{L}^2(\Gamma_{I_n})\times\mathbf{L}^2(\Gamma_{I_n})} \,, \tag{3.4}$$

where $\mathbf{h}^n = \mathbf{g}^n - \overline{\mathbf{g}}^n$. Hence, starting with arbitrary $\mathbf{g}^n_{(0)}$, we can find a sequence $\{\mathbf{g}^n_{(k)}\}$ obtained by $\mathbf{g}^n_{(k)} = \mathbf{g}^n_{(k-1)} + \mathbf{h}^n_{(k)}$, where $\mathbf{h}^n_{(k)}$ is a solution of the linear least squares problem (3.4).

Following is the definition of the linearized and linear adjoint problems that are to be solved in the use of the conjugate gradient algorithm and Algorithm 3.3. The linearized and linear adjoint problems are presented along with a proof of the definition of the adjoint for the first and second order structure formulations in sections 3.1 and 3.2, respectively.

3.1 First Order Time Discretization of the Structure Subsystem

For $\overline{\mathbf{g}}^n \in \mathbf{L}^2(\Gamma_{I_n})$, the Fréchet derivative $N'(\overline{\mathbf{g}}^n)(\cdot) : \mathbf{L}^2(\Gamma_{I_n}) \to \mathbf{L}^2(\Gamma_{I_n}) \times \mathbf{L}^2(\Gamma_{I_n})$ is defined by

$$N'_n(\overline{\mathbf{g}}^n)(\mathbf{h}^n) = \begin{pmatrix} (\mathbf{w}^n - \frac{\boldsymbol{\phi}^n \circ \Psi_n^{-1}}{\Delta t}) \mid_{\Gamma_{I_n}} \\ \sqrt{\epsilon}\, \mathbf{h}^n \end{pmatrix},$$

where $\mathbf{w}^n$, $\boldsymbol{\phi}^n$ are the solutions of

$$\begin{aligned} &\rho_f(\mathbf{w}^n, \mathbf{v})_{\Omega^f_{t_n}} + \Delta t\, \rho_f \Big[(\mathbf{w}^n \cdot \nabla \overline{\mathbf{u}}^n, \mathbf{v})_{\Omega^f_{t_n}} + ((\overline{\mathbf{u}}^n - \mathbf{z}^n) \cdot \nabla \mathbf{w}^n, \mathbf{v})_{\Omega^f_{t_n}} \\ &\quad -(\mathbf{w}^n (\nabla \cdot \mathbf{z}^n), \mathbf{v})_{\Omega^f_{t_n}}\Big] + \Delta t \left[2\nu_f (D(\mathbf{w}^n),\, D(\mathbf{v}))_{\Omega^f_{t_n}} - (\psi^n, \nabla \cdot \mathbf{v})_{\Omega^f_{t_n}}\right] \\ &= \Delta t\, (\mathbf{h}^n, \mathbf{v})_{\Gamma_{I_n}} \ \forall \mathbf{v} \in \mathbf{U}_{t_n}\,, \end{aligned} \tag{3.5}$$

$$(q, \nabla \cdot \mathbf{w}^n)_{\Omega^f_{t_n}} = 0 \quad \forall q \in Q_{t_n}\,, \tag{3.6}$$

and

$$\begin{aligned} \rho_s\, (\boldsymbol{\phi}^n, \boldsymbol{\xi})_{\Omega^s} + \Delta t^2\, [2\, \nu_s\, (D(\boldsymbol{\phi}^n), D(\boldsymbol{\xi}))_{\Omega^s} + \lambda\, (\nabla \cdot \boldsymbol{\phi}^n, \nabla \cdot \boldsymbol{\xi})_{\Omega^s}] \\ = -\Delta t^2 (\mathbf{h}^n, \boldsymbol{\xi} \circ \Psi_n^{-1})_{\Gamma_{I_n}} \ \forall \boldsymbol{\xi} \in \boldsymbol{\Sigma}\,, \end{aligned} \tag{3.7}$$

where $\overline{\mathbf{u}}^n$ is the solution of (2.27)-(2.28) with $\mathbf{g}^n$ replaced by $\overline{\mathbf{g}}^n$.

It is necessary to define the adjoint operator of $N'_n(\overline{\mathbf{g}}^n)$ in order to solve the linear least squares problem (3.4).

Theorem 3.1 *The adjoint of* $(N'_n(\overline{\mathbf{g}}^n))(\cdot)$ *is* $(N'_n(\overline{\mathbf{g}}^n))^*(\cdot) : \mathbf{L}^2(\Gamma_{I_n}) \times \mathbf{L}^2(\Gamma_{I_n}) \to \mathbf{L}^2(\Gamma_{I_n})$, *given by*

$$(N'_n(\overline{\mathbf{g}}_n))^* \begin{pmatrix} \mathbf{r}^n \\ \mathbf{s}^n \end{pmatrix} = (\boldsymbol{\beta}^n - \frac{\boldsymbol{\varphi}^n \circ \Psi_n^{-1}}{\Delta t})|_{\mathbf{L}^2(\Gamma_{I_n})} + \sqrt{\epsilon}\, \mathbf{s}^n\,,$$

where $\boldsymbol{\beta}^n$, $\boldsymbol{\varphi}^n$ *are the solutions of*

$$\begin{aligned} &\rho_f(\boldsymbol{\beta}^n, \mathbf{v})_{\Omega^f_{t_n}} + \Delta t\, \rho_f \Big[(\mathbf{v} \cdot \nabla \overline{\mathbf{u}}^n, \boldsymbol{\beta}^n)_{\Omega^f_{t_n}} + ((\overline{\mathbf{u}}^n - \mathbf{z}^n) \cdot \nabla \mathbf{v}, \boldsymbol{\beta}^n)_{\Omega^f_{t_n}} \\ &\quad -(\boldsymbol{\beta}^n (\nabla \cdot \mathbf{z}^n), \mathbf{v})_{\Omega^f_{t_n}}\Big] + \Delta t \left[2\nu_f (D(\boldsymbol{\beta}^n),\, D(\mathbf{v}))_{\Omega^f_{t_n}} - (\alpha^n, \nabla \cdot \mathbf{v})_{\Omega^f_{t_n}}\right] \\ &= \Delta t\, (\mathbf{r}^n, \mathbf{v})_{\Gamma_{I_n}} \ \forall \mathbf{v} \in \mathbf{U}_{t_n}\,, \end{aligned} \tag{3.8}$$

$$(q, \nabla \cdot \boldsymbol{\beta}^n)_{\Omega^f_{t_n}} = 0 \quad \forall q \in Q_{t_n}\,, \tag{3.9}$$

and

$$\rho_s\,(\boldsymbol{\varphi}^n,\boldsymbol{\xi})_{\Omega^s} + \Delta t^2\,\left[2\,\nu_s\,(D(\boldsymbol{\varphi}^n),D(\boldsymbol{\xi}))_{\Omega^s} + \lambda\,(\nabla\cdot\boldsymbol{\varphi}^n,\nabla\cdot\boldsymbol{\xi})_{\Omega^s}\right] = -\Delta t^2\,(\mathbf{r}^n,\boldsymbol{\xi}\circ\Psi_n^{-1})_{\Gamma_{I_n}}\;\forall\boldsymbol{\xi}\in\boldsymbol{\Sigma}\,. \tag{3.10}$$

Note that the the linearized structure subsystem is self-adjoint. Again, $\overline{\mathbf{u}}^n$ in (3.8) is the solution of (2.27)–(2.28) with the replacement of $\mathbf{g}^n$ by $\overline{\mathbf{g}}^n$.

Proof: Let $(\mathbf{v},q)=(\boldsymbol{\beta}^n,\alpha^n)$ and $\boldsymbol{\xi}=\boldsymbol{\varphi}^n$ in (3.5)-(3.7). Also, let $(\mathbf{v},q)=(\mathbf{w}^n,\psi^n)$ and $\boldsymbol{\xi}=\boldsymbol{\phi}^n$ in (3.8)-(3.10). From this, we obtain that $(\mathbf{h}^n,\boldsymbol{\varphi}^n\circ\Psi_n^{-1})_{\Gamma_{I_n}} = (\mathbf{r}^n,\boldsymbol{\phi}^n\circ\Psi_n^{-1})_{\Gamma_{I_n}}$ and $(\mathbf{h}^n,\boldsymbol{\beta}^n)_{\Gamma_{I_n}} = (\mathbf{r}^n,\mathbf{w}^n)_{\Gamma_{I_n}}$. Therefore,

$$\begin{aligned}\left(N_n'(\overline{\mathbf{g}}^n)\mathbf{h}^n,\begin{bmatrix}\mathbf{r}^n\\ \mathbf{s}^n\end{bmatrix}\right) &= (\mathbf{w}^n-\frac{\boldsymbol{\phi}^n\circ\Psi_n^{-1}}{\Delta t},\mathbf{r}^n)_{\Gamma_{I_n}} + \sqrt{\epsilon}(\mathbf{h}^n,\mathbf{s}^n)_{\Gamma_{I_n}}\\ &= (\mathbf{h}^n,\boldsymbol{\beta}^n-\frac{\boldsymbol{\varphi}^n\circ\Psi_n^{-1}}{\Delta t})_{\Gamma_{I_n}} + \sqrt{\epsilon}(\mathbf{h}^n,\mathbf{s}^n)_{\Gamma_{I_n}}\\ &= \left(\mathbf{h}^n,N_n'(\overline{\mathbf{g}}^n)^*\left(\begin{bmatrix}\mathbf{r}^n\\ \mathbf{s}^n\end{bmatrix}\right)\right).\end{aligned}$$

□

3.2 Second Order Time Discretization of the Structure Subsystem

For $\overline{\mathbf{g}}^n\in\mathbf{L}^2(\Gamma_{I_n})$, the Fréchet derivative $N'(\overline{\mathbf{g}}^n)(\cdot):\mathbf{L}^2(\Gamma_{I_n})\to\mathbf{L}^2(\Gamma_{I_n})\times\mathbf{L}^2(\Gamma_{I_n})$ is defined by

$$N_n'(\overline{\mathbf{g}}^n)(\mathbf{h}^n)=\begin{pmatrix}(\mathbf{w}^n-\dot{\boldsymbol{\phi}}^n\circ\Psi_n^{-1})\mid_{\Gamma_{I_n}}\\ \sqrt{\epsilon}\,\mathbf{h}^n\end{pmatrix},$$

where $\mathbf{w}^n$ is the solution of (3.5)-(3.6), and $\boldsymbol{\phi}^n$ is the solution of

$$\begin{aligned}&\rho_s\left(\dot{\boldsymbol{\phi}}^n,\boldsymbol{\xi}\right)_{\Omega^s} + \Delta t\,\left[\nu_s\,(D(\boldsymbol{\phi}^n),D(\boldsymbol{\xi}))_{\Omega^s} + \frac{\lambda}{2}\,(\nabla\cdot\boldsymbol{\phi}^n,\nabla\cdot\boldsymbol{\xi})_{\Omega^s}\right]\\ &\qquad = -\Delta t(\mathbf{h}^n,\boldsymbol{\xi}\circ\Psi_n^{-1})_{\Gamma_{I_n}}\;\forall\boldsymbol{\xi}\in\boldsymbol{\Sigma}\,,\\ &(\boldsymbol{\phi}^n,\boldsymbol{\gamma})_{\Omega^s} - \frac{\Delta t}{2}\left(\dot{\boldsymbol{\phi}}^n,\boldsymbol{\gamma}\right)_{\Omega^s} = 0\;\forall\boldsymbol{\gamma}\in\boldsymbol{\Sigma}\,.\end{aligned} \tag{3.11}$$

We now define the adjoint operator of $N_n'(\overline{\mathbf{g}}^n)$ needed in order to solve the linear least squares problem (3.4).

Theorem 3.2 *The adjoint of* $(N_n'(\overline{\mathbf{g}}^n))(\cdot)$ *is* $(N_n'(\overline{\mathbf{g}}^n))^*(\cdot):\mathbf{L}^2(\Gamma_{I_n})\times\mathbf{L}^2(\Gamma_{I_n})\to\mathbf{L}^2(\Gamma_{I_n})$, *given by*

$$(N_n'(\overline{\mathbf{g}}_n))^*\begin{pmatrix}\mathbf{r}^n\\ \mathbf{s}^n\end{pmatrix} = (\boldsymbol{\beta}^n-\boldsymbol{\varphi}^n\circ\Psi_n^{-1})|_{\mathbf{L}^2(\Gamma_{I_n})} + \sqrt{\epsilon}\,\mathbf{s}^n\,,$$

where $\boldsymbol{\beta}^n$ is the solution of (3.8)-(3.9) and $\boldsymbol{\varphi}^n$ is the solution of

$$(\dot{\boldsymbol{\varphi}}^n, \boldsymbol{\xi})_{\Omega^s} + \Delta t \left[\nu_s \left(D(\boldsymbol{\varphi}^n), D(\boldsymbol{\xi}) \right)_{\Omega^s} + \frac{\lambda}{2} \left(\nabla \cdot \boldsymbol{\varphi}^n, \nabla \cdot \boldsymbol{\xi} \right)_{\Omega^s} \right] = 0 \; \forall \boldsymbol{\xi} \in \boldsymbol{\Sigma} \,, \quad (3.12)$$

$$\rho_s \left(\boldsymbol{\varphi}^n, \boldsymbol{\gamma} \right)_{\Omega^s} - \frac{\Delta t}{2} \left(\dot{\boldsymbol{\varphi}}^n, \boldsymbol{\gamma} \right)_{\Omega^s} = -\Delta t \left(\mathbf{r}^n, \boldsymbol{\gamma} \circ \Psi_n^{-1} \right)_{\Gamma_{I_n}} \; \forall \boldsymbol{\gamma} \in \boldsymbol{\Sigma} \,. \quad (3.13)$$

Proof: Let $(\mathbf{v}, q) = (\boldsymbol{\beta}^n, \alpha^n)$ and $(\boldsymbol{\xi}, \boldsymbol{\gamma}) = (\boldsymbol{\varphi}^n, \dot{\boldsymbol{\varphi}^n})$ in (3.5)-(3.6) and (3.11)-(3.11). Also, let $(\mathbf{v}, q) = (\mathbf{w}^n, \psi^n)$ and $(\boldsymbol{\xi}, \boldsymbol{\gamma}) = (\boldsymbol{\phi}^n, \dot{\boldsymbol{\phi}^n})$ in (3.8)-(3.9) and (3.12)-(3.13). From this, we obtain that $(\mathbf{h}^n, \boldsymbol{\varphi}^n \circ \Psi_n^{-1})_{\Gamma_{I_n}} = (\mathbf{r}^n, \dot{\boldsymbol{\phi}^n} \circ \Psi_n^{-1})_{\Gamma_{I_n}}$ and $(\mathbf{h}^n, \boldsymbol{\beta}^n)_{\Gamma_{I_n}} = (\mathbf{r}^n, \mathbf{w}^n)_{\Gamma_{I_n}}$.

Therefore,

$$\begin{aligned} \left(N_n'(\overline{\mathbf{g}}^n)\mathbf{h}^n, \begin{bmatrix} \mathbf{r}^n \\ \mathbf{s}^n \end{bmatrix} \right) &= (\mathbf{w}^n - \dot{\boldsymbol{\phi}^n} \circ \Psi_n^{-1}, \mathbf{r}^n)_{\Gamma_{I_n}} + \sqrt{\epsilon} (\mathbf{h}^n, \mathbf{s}^n)_{\Gamma_{I_n}} \\ &= (\mathbf{h}^n, \boldsymbol{\beta}^n - \boldsymbol{\varphi}^n \circ \Psi_n^{-1})_{\Gamma_{I_n}} + \sqrt{\epsilon} (\mathbf{h}^n, \mathbf{s}^n)_{\Gamma_{I_n}} \\ &= \left(\mathbf{h}^n, N_n'(\overline{\mathbf{g}}^n)^* \left(\begin{bmatrix} \mathbf{r}^n \\ \mathbf{s}^n \end{bmatrix} \right) \right) . \end{aligned}$$

□

3.3 Algorithm

We adopt the conjugate gradient algorithm for the linear least squares problem (3.4), which can be found in many references [13, 14, 15]. For the algorithm, we adopt the notation $A = N_n'(\overline{\mathbf{g}}^n)$, $A^* = (N_n'(\overline{\mathbf{g}}^n))^*$, $b = -N_n(\overline{\mathbf{g}}^n)$, and $x = \mathbf{h}^n$.

The nonlinear least squares problem (3.3) can be solved using the following Gauss-Newton algorithm.

Algorithm 3.3

1. *Choose* $\mathbf{g}_{(0)}^n$.
2. *For* $k = 1, 2, 3, \ldots,$
   a. *computable in parallel:*
      i. *find* $\mathbf{u}_{(k)}^n$ *and* $p_{(k)}^n$ *on* $\Omega_{t_n,(k-1)}^f$ *using* $\mathbf{z}_{(k-1)}^n$ *and* $\mathbf{g}_{(k-1)}^n$,
      ii. *find* $\boldsymbol{\eta}_{(k)}^n$ *and* $\dot{\boldsymbol{\eta}}_{(k)}^n$ *using* $\mathbf{g}_{(k-1)}^n$,
   b. *update* $\Gamma_{I_n^{(k)}}$, $\mathbf{z}_{(k)}^n$, $\Psi_n^{(k)}$, *and* $\Omega_{t_n,(k)}^f$ *using* $\boldsymbol{\eta}_{(k)}^n$,
   c. *if* $\frac{1}{2} \int_{\Gamma_{I_n^{(k-1)}}} |\mathbf{u}^n - \dot{\boldsymbol{\eta}}^n \circ (\Psi_n^{(k-1)})^{-1}|^2 \, d\Gamma \; < \; \epsilon_{tol}$, *break,*
   d. *compute* $\mathbf{h}_{(k)}^n$ *by the conjugate gradient algorithm with* $A = N_n'(\mathbf{g}_{(k-1)}^n)$, $b = -N_n(\mathbf{g}_{(k-1)}^n)$, *and* $x = \mathbf{h}_{(k)}^n$,

e. set $\mathbf{g}^n_{(k)} = \mathbf{g}^n_{(k-1)} + \mathbf{h}^n_{(k)}$.

Remark 3.4 *Our choice of* $\mathbf{g}^n_{(0)}$ *in step 1. of Algorithm 3.3 is the final value of* $\mathbf{g}^{n-1}$ *determined in the previous time step.*

Remark 3.5 *In step 2.d. of Algorithm 3.3, determining* $\mathbf{h}^n_{(k)}$ *by means of the conjugate gradient algorithm is accomplished on the moving fluid domain determined by the structure problem using the control* $\mathbf{g}^n_{(k-1)}$. *Therefore, the moving fluid domain must only be updated for each Gauss-Newton iteration of Algorithm 3.3.*

4 Numerical Results

4.1 Haemodynamic Experiment

The first of two numerical tests is an FSI problem using the ALE formulation for the moving fluid domain, reported in [18], using parameters that are consistent with blood flow in a human body. The problem is heavily affected by the added mass effect, since the densities of the fluid and structure are very close, and is therefore an excellent test candidate. This effect causes explicit decoupling without relaxation to fail, as was observed by experimentation and also reported in [18].

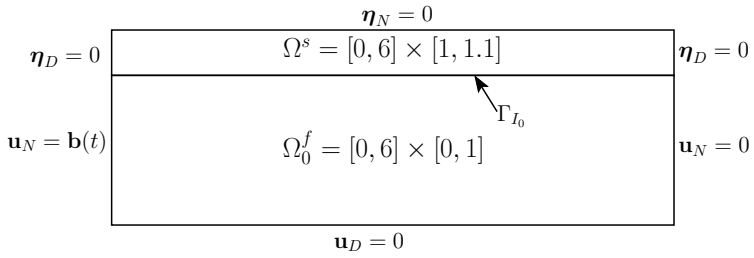

Figure 2: Domain and boundary conditions for numerical experiment

A force $\mathbf{b}(t)$ is applied to the left fluid boundary (Fig. 2) at t s where

$$\mathbf{b}(t) = \begin{cases} (-10^3(1-\cos\frac{2\pi t}{.025}),0) \ \text{ dyne/cm}^2, & t \le 0.025 \\ (0,0), & 0.025 < t < T. \end{cases}$$

The function $\mathbf{b}(t)$ defines the stress on the inlet denoted by $\mathbf{u}_N$ in (2.4). The volume force for the fluid and structure are $\mathbf{f}(t) = (0,0)$ dyne/cm^2. The other boundary conditions on the domain configuration are homogeneous Dirichlet or Neumann (Fig. 2), and the simulation begins at rest.

The reference domain for the fluid subsystem has height 1 cm and length 6 cm. The density of the fluid, ρ_f, is 1 g/cm^3 and the viscosity of the fluid, ν_f, is 0.035 g/cm·s. The structure domain has height 0.1 cm and length 6 cm. The density of the structure, ρ_s, is 1.1 g/cm^3. The Young's Modulus of the structure, E, is 3×10^6 dyne/cm^2 and its Poisson ratio, ν, is 0.3. The Lamé-Navier parameters λ and ν_s are defined as follows:

$$\lambda = \frac{\nu E}{(1-2\nu)(1+\nu)} \text{ dyne/cm}^2, \quad \nu_s = \frac{E}{2(1+\nu)} \text{ dyne/cm}^2.$$

The fluid and structure reference domains were spatially discretized using a uniform mesh. Let h_x and h_y represent the spatial discretization in the x and y direction, respectively. We used the triangular $(\mathbb{P}_1 + bubble, \mathbb{P}_1)$ pair for the finite element solution to (2.27)-(2.28) on the fluid domain and $\mathbb{P}_1$ finite elements for the solution to (2.29) or (2.30)-(2.31) on the structure domain for all computations that will be presented. Additionally, all computations performed used a time step of $\Delta t = 10^{-4}$ s and were from 0 s until $T = 0.1$ s. All computations were performed using FreeFEM++ [21].

The first sequence of simulations (Fig. 3) demonstrates the strong dependence of the solution on the spatial discretization. The plots of the vertical displacement on the interface are computed using Algorithm 3.3. Worth noting is that using a spatial discretization with $h_x = 0.1$ cm and allowing h_y to range from 0.1 cm to $\frac{1}{30}$ cm for both computational domains gives significantly different results. There is much more agreement using the two finer spatial discretizations which indicates that the solution is sensitive to having degrees of freedom on the interior of the structure FEM space.

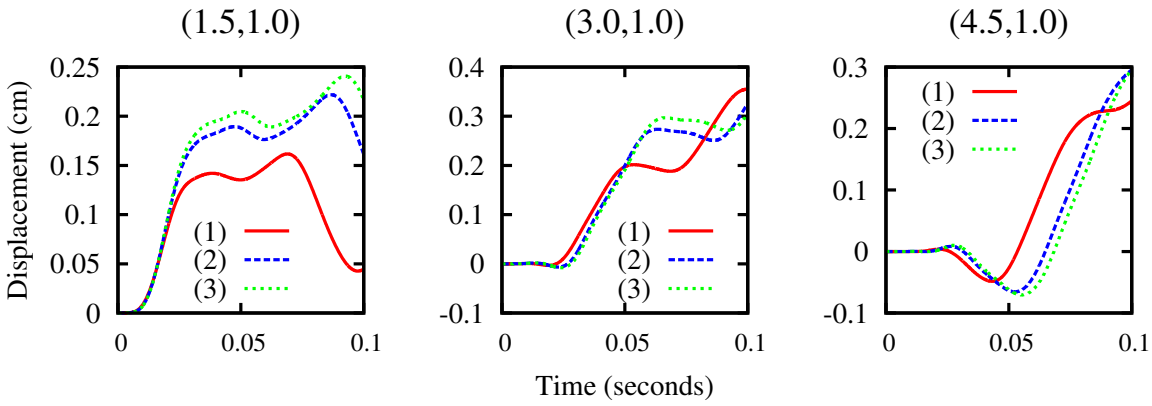

Figure 3: Vertical displacement at three points on the interface using the first order structure formulation with: (1) $h_x = 0.1$ cm, $h_y = 0.1$ cm, (2) $h_x = 0.1$ cm, $h_y = 0.05$ cm, and (3) $h_x = 0.1$ cm, $h_y = \frac{1}{30}$ cm

The solution to the FSI problem computed by Murea and Sy [18] is on a mesh with $h_x \approx 0.2$ cm and $h_y \approx 0.1$ cm for the structure domain, $h_x \approx 0.1$ cm and $h_y \approx 0.1$ cm for the fluid domain. We have seen that the solution depends heavily on spatial discretization with a mesh as coarse as is used for this comparison, so it is not reasonable for us to expect an exact match with their results. Particularly because, in Murea and Sy's work, a truncated eigenfunction basis for the solution on the structure domain was used. Additionally, the uniqueness of the optimal solution is not guaranteed theoretically for Algorithm 3.3 in its continuous form, so the numerical solution may be determined by the initial choice of the control. Regardless, we have compared our solution with Murea and Sy's (Fig. 4) and note that, while they differ in amplitude, they both have similar wavelike features. Our computation was made using $h_x = 0.2$ cm and $h_y = 0.1$ cm for the structure domain, $h_x = 0.1$ cm and $h_y = 0.1$ cm for the fluid domain, $\epsilon = 0$, and $\epsilon_{tol} = 10^{-6}$ for Algorithm 3.3.

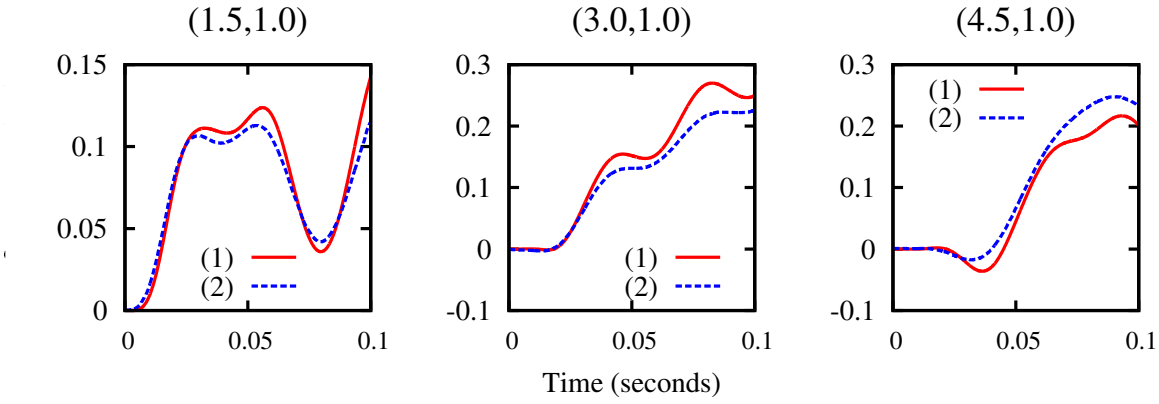

Figure 4: Vertical displacement at three points on the interface using Algorithm 3.3 with the first order formulation for the structure (1) beside the vertical displacement from Murea and Sy (2)

Table 4.1 contains the norm of the jump in velocities on the interface at three time steps for the computation made using $h_x = 0.05$ cm and $h_y = 0.05$ cm as the spatial discretization, $\epsilon = 0$, and $\epsilon_{tol} = 10^{-6}$. Please observe the fast convergence of the Gauss-Newton iterations. Figure 5 contains pressure profiles of the same solution at the same three time steps.

Interface Velocity Error $\mathcal{J}_n(\cdot)$

Time (s)	Iter. 1	Iter. 2	Iter. 3
0.010	4.1781e-04	5.7408e-05	6.2945e-08
0.025	1.4958e-04	1.4712e-04	2.6601e-08
0.035	2.3213e-04	1.0033e-04	1.4864e-09

Table 1: Error in the continuity of velocity between subsystems for each Gauss-Newton iteration at three representative time steps

We now verify that the solutions found by Algorithm 3.3 for the first and second order formulations of the linear elastic structure closely match the solution found with Aitken's relaxation [8], using the same finite elements and with the same spatial discretization. Aitken's relaxation is an implicit scheme that is applied to the structure update. It works by relaxing the update to $\boldsymbol{\eta}^n$ at each iteration of an implicit scheme. For instance, suppose $\tilde{\boldsymbol{\eta}}^n_{(k)}$ is the solution to the structure subproblem for implicit iteration k. Then, $\boldsymbol{\eta}^n_{(k)}$ is updated as

$$\boldsymbol{\eta}^n_{(k)} = \omega\, \tilde{\boldsymbol{\eta}}^n_{(k)} + (1-\omega)\, \boldsymbol{\eta}^n_{(k-1)},\ \omega \in (0,1]. \tag{4.14}$$

See [8] for more details on Aitken's relaxation.

While easy to implement, this is an incredibly expensive method to use because ω must be very small in order the system to remain stable and converge. The smaller the value of ω, the more iterations are needed at each time step, requiring many nonlinear solves on the fluid domain. Using $\omega = 0.025$, the result is reliable and useful as a reference solution with

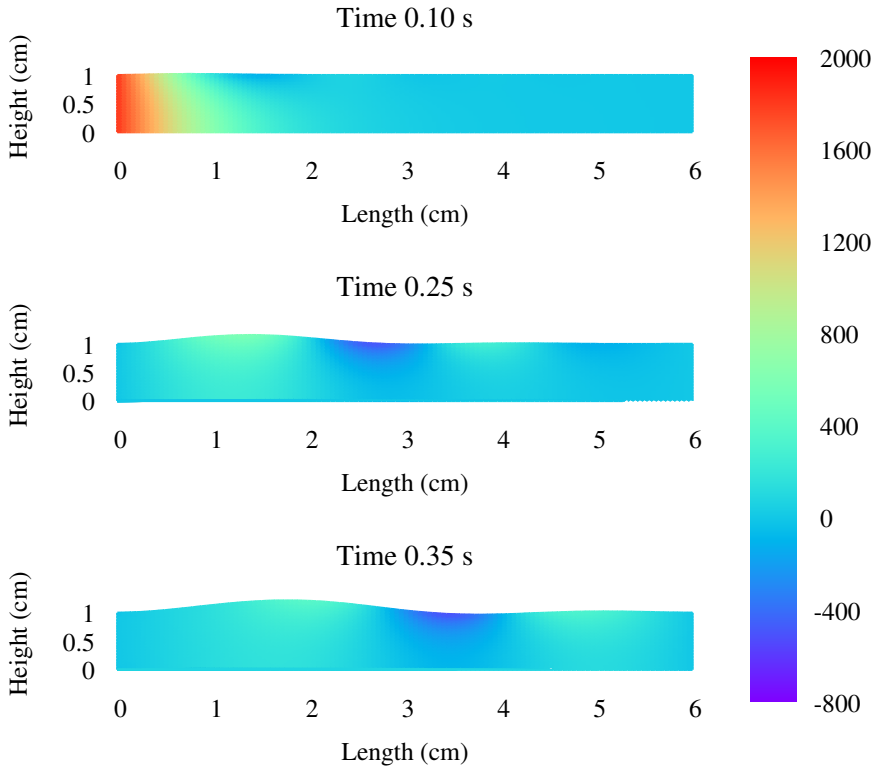

Figure 5: Fluid pressure profiles [dyne/cm^2] at three time steps

which to compare (Fig. 6). Spatial discretization was made with $h_x = 0.2$ cm and $h_y = 0.1$ cm for both fluid and structure domains. The stopping criteria used for Aitken's relaxation was $\left(\int_{\Gamma_{I_0}} (\boldsymbol{\eta}^n_{(k)} - \boldsymbol{\eta}^n_{(k-1)})^2 \, d\Gamma\right)^{\frac{1}{2}} < 10^{-7}$, while $\epsilon = 0$ and $\epsilon_{tol} = 10^{-6}$ for Algorithm 3.3.

It was observed that the first and second order formulation for the structure made no significant difference on the solution found. Both solutions matched well the reference result using Aitken's relaxation, and as expected, Algorithm 3.3 significantly reduced computation times. The first order formulation using Algorithm 3.3 ran for 135 minutes before completion, while the Aitken's relaxation ran for 1624 minutes with a tolerance of 10^{-6} on each time step and 2701 minutes using a tolerance of 10^{-7} on each time step. We do not expect a 90% reduction in run time compared with other state-of-the-art implicit methods, but Aitkens relaxation is a benchmark against which many implicit algorithms can be compared.

4.2 Comparison with an analytical solution

In order to observe the convergence and accuracy of our method, we have compared it with the analytical solution for the FSI problem presented by Astorino and Grandmont [2]. The fluid governing equations are for Stokes flow on a stationary fluid domain, but still have

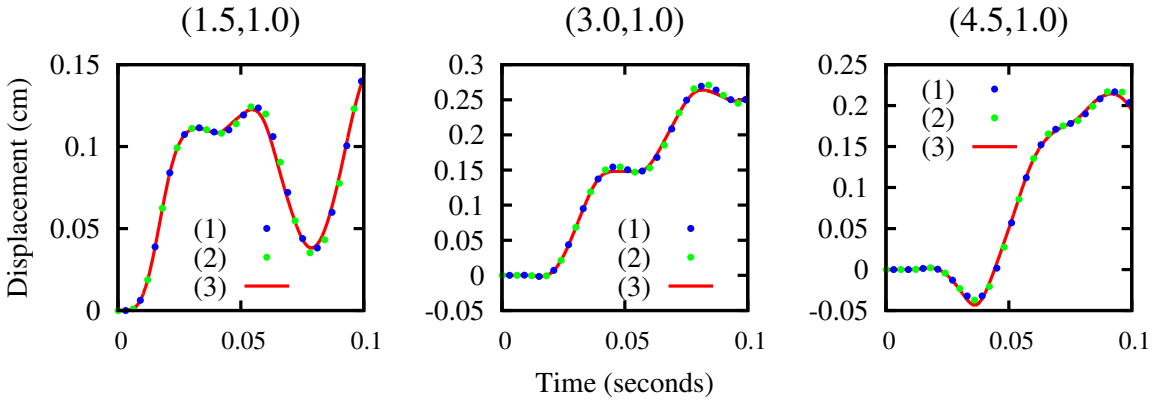

Figure 6: Vertical displacement at three points on the interface using first (1) and second (2) order formulations with the optimal control algorithm beside vertical displacement using Aitken's relaxation (3)

the same challenge of solving an FSI problem with similar densities between the fluid and structure [1, 3, 6]. This problem also provides support that our optimal control approach is applicable for solving a broad range of FSI problems. Solving the Stokes flow on a stationary domain means that when we solve (2.27)-(2.28), the equations will not have the nonlinear term $(\mathbf{u}^n, \mathbf{u}^n, \mathbf{v})_{\Omega^f_{t_n}}$ and we will drop all terms including $\mathbf{z}$, since $\mathbf{z} = 0$ and $\nabla \cdot \mathbf{z} = 0$ in the Eulerian framework. The corresponding terms are removed from the linearized and adjoint problems defined in sections 3.1 and 3.2.

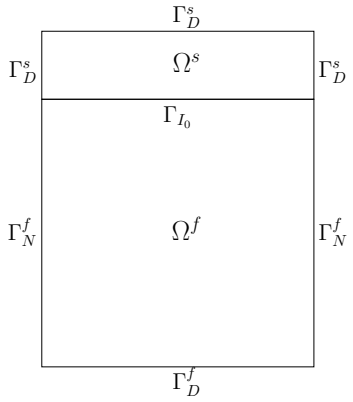

Figure 7: Computational domain

Parameters for the problem are: $\rho_f = 1.0$ g/cm^3, $\nu_f = 0.0013$ g/cm·s, $\rho_s = 1.9$ g/cm^3, $\nu_s = 3$ dyne/cm^2, and $\lambda = 4.5$ dyne/cm^2. Initial conditions, body forces, and boundary conditions are determined by the analytical solution in order for the solution to the coupled problem to be the analytical solution:

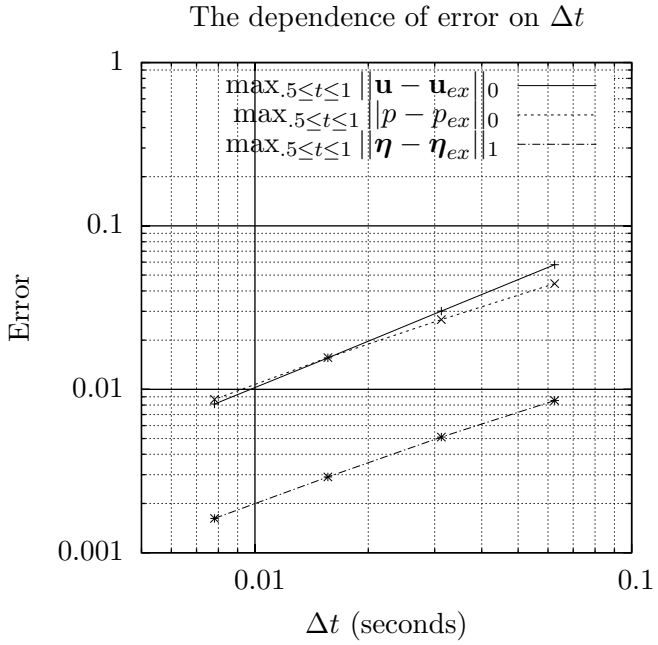

Figure 8: Convergence results for the analytic problem

On $\Omega_t^f = \Omega^f = [0,1] \times [0,1]$ and $\Omega^s = [0,1] \times [1,1.25]$ (Fig. 7),

$$\begin{aligned}
\mathbf{u}_1 &= \cos(x+t)\sin(y+t) + \sin(x+t)\cos(y+t), \\
\mathbf{u}_2 &= -\sin(x+t)\cos(y+t) - \cos(x+t)\sin(y+t), \\
p &= 2\nu_f(\sin(x+t)\sin(y+t) - \cos(x+t)\cos(y+t)) + 2\nu_s \cos(x+t)\sin(y+t), \\
\boldsymbol{\eta}_1 &= \sin(x+t)\sin(y+t), \\
\boldsymbol{\eta}_2 &= \cos(x+t)\cos(y+t). \qquad (4.15)
\end{aligned}$$

As in [2], we used a uniform mesh with a spatial discretization of $h = 0.05$ cm. The Taylor-Hood finite element pair, $(\mathbb{P}_2, \mathbb{P}_1)$, were used for solutions on the fluid domain, while $\mathbb{P}_2$ finite elements were used to approximate the structure displacement. The FSI problem was repeatedly solved by Algorithm 3.3 using decreasing timesteps ($\Delta t = 6.25 \cdot 10^{-2}, 3.125 \cdot 10^{-2}, 1.5625 \cdot 10^{-2}, 7.8125 \cdot 10^{-3}$ s) and compared with the exact solution (4.15). For Algorithm 3.3, $\epsilon = 0$ and $\epsilon_{tol} = 10^{-6}$. Norms used to compute the error between the solution found by means of our optimal control algorithm and the exact solution are as follows: for $\mathbf{u}$ and p, $\mathbf{L}^\infty(0.5, 1, \mathbf{L}^2(\Omega^f))$; for $\boldsymbol{\eta}$, $\mathbf{L}^\infty(0.5, 1, \mathbf{H}^1(\Omega^s))$. Results are plotted in logarithmic scale format as a function of Δt in Figure 8 and are approximately linear. The results indicate that our algorithm for solving the FSI problem converges upon the exact solution. Providing error estimation for the optimal control algorithm will be the focus of future research, but is not within the scope of this paper.

5 Conclusion

The fluid-structure interaction problem was formulated as an optimal control problem where violation of continuity of velocity on the interface of two subsystems is minimized using a

common stress along the interface as a control. Our algorithm has successfully decoupled the FSI problem into two subproblems. Very few nonlinear solves are needed for each time step because of the fast convergence of the Gauss-Newton algorithm in determining the optimal stress control. It was not necessary to introduce relaxation parameters for updating either the structure or fluid subsystems. Additionally, all problems including the linearized and adjoint problems for the fluid and structure subsystem can be solved in parallel, which is increasingly important as more effort is being expended on building large computational clusters for distributed computing.

Although Figure 3 indicates that the solution to the first FSI problem tested was very sensitive to spatial discretization and finite element choice, our algorithm was able to find solutions that enforced continuity of stress always and continuity of velocity within a specified tolerance. Further, Figure 6 indicates that the solution of the optimization algorithm matched the results of using a much more computationally expensive implicit method and also shows very strong agreement between both first and second order formulations for the structure subproblem. Computation time was reduced by over 90% when compared with a naive but easy to implement Aitken's relaxation method.

Using a Stokes-linear elastic structure FSI problem on a fixed domain with an analytical solution, we were able to show nearly linear convergence in the very strict $||\cdot||_{\mathbf{L}^\infty}$ norm with respect to time. This gives us confidence that the algorithm by optimization is converging upon the true solution.

Our approach is not specific to the fluid or structure subsystems, beyond finding the Fréchet derivative and adjoint operator. We look to apply this method in future work to both nonlinear structures and Non-Newtonian fluids, as well as provide further analysis in the framework of optimal control.

References

[1] M. Astorino, F. Chouly, M.A. Fernández, Robin Based Semi-Implicit Coupling in Fluid-Structure Interaction: Stability Analysis and Numerics, SIAM Journal on Scientific Computing. 31 (2009) 4041-4065.

[2] M. Astorino, C. Grandmont, Convergence analysis of a projection semi-implicit coupling scheme for fluid-structure interaction problems, Numerische Mathematik. 116 (2010) 721-767.

[3] S. Badia, F. Nobile, C. Vergara, Fluid-structure partitioned procedures based on Robin transmission conditions, Journal of Computational Physics. 227 (2008) 7027-7051.

[4] Y. Bazilevs, V.M. Calo, T.J.R. Hughes, Y. Zhang, Isogeometric fluid-structure interaction: theory, algorithms, and computations, Computational Mechanics. 43 (2008) 3-37.

[5] J. Boujot, Mathematical formulation of fluid-structure interaction problems, ESAIM: Mathematical Modelling and Numerical Analysis. 21 (1987) 239-260.

[6] E. Burman, M.A. Fernández, Stabilization of explicit coupling in fluid-structure interaction involving fluid incompressibility, Computer Methods in Applied Mechanics and Engineering. 198 (2009) 766-784.

[7] S. Čanić, A. Mikelić, J. Tambača, A two-dimensional effective model describing fluid-structure interaction in blood flow: analysis, simulation and experimental validation, Fluid-solid Interactions: Modeling, Simulation, Bio-mechanical Applications. 333 (2005) 867-883.

[8] P. Causin, J.-F. Gerbeau, F. Nobile, Added-mass effect in the design of partitioned algorithms for fluid-structure problems, BANG - INRIA Rocquencourt, 2004.

[9] J. Chrispell, L. Fauci, Peristaltic Pumping of Solid Particles Immersed in a Viscoelastic Fluid, Mathematical Modelling of Natural Phenomena. 6 (2011) 67-83.

[10] J. Donea, S. Giuliani, J.P. Halleux, An arbitrary lagrangian-eulerian finite element method for transient dynamic fluid-structure interactions, Computer Methods in Applied Mechanics and Engineering. 33 (1982) 689-723.

[11] V.J. Ervin, E.W. Jenkins, H. Lee, Approximation of the Stokes-Darcy System by Optimization, Journal of Scientific Computing. (2013). <http://dx.doi.org/10.1007/s10915-013-9779-8>.

[12] L. Formaggia, F. Nobile, Stability analysis for the arbitrary Lagrangian Eulerian formulation with finite elements, East-West Journal of Numerical Mathematics. 7 (1999) 105-131.

[13] G.H. Golub, C.F. Van Loan, Matrix computations, Johns Hopkins University Press, Baltimore, 1989.

[14] C.W. Groetsch, Generalized Inverses of Linear Operators: Representation and Approximation, M. Dekker, New York, 1977.

[15] M. Gunzburger, H. Lee, An Optimization-Based Domain Decomposition Method for the Navier–Stokes Equations, SIAM Journal on Numerical Analysis. 37 (2000) 1455-1480.

[16] J.J. Heys, T.A. Manteuffel, S.F. McCormick, J.W. Ruge, First-order system least squares (FOSLS) for coupled fluid-elastic problems, Journal of Computational Physics. 195 (2004) 560-575.

[17] U. Küttler, W.A. Wall, Fixed-point fluid-structure interaction solvers with dynamic relaxation, Computational Mechanics. 43 (2008) 61-72.

[18] C.M. Murea, S. Sy, A fast method for solving fluid-structure interaction problems numerically, International Journal for Numerical Methods in Fluids. 60 (2009) 1149-1172.

[19] F. Nobile, C. Vergara, An Effective Fluid-Structure Interaction Formulation for Vascular Dynamics by Generalized Robin Conditions, SIAM Journal on Scientific Computing. 30 (2008) 731-763.

[20] R.G. Owens, T.N. Phillips, Computational rheology, Imperial College Press, London, 2002.

[21] O. Pironneau, F. Hecht, A.L. Hyaric, K. Ohtsuka, FreeFEM, www.freefem.org, (2013).

[22] A. Quarteroni, M. Tuveri, A. Veneziani, Computational vascular fluid dynamics: problems, models and methods, Computing and Visualization in Science. 2 (2000) 163-197.

[23] K.P. Selverov, H.A. Stone, Peristaltically driven channel flows with applications toward micromixing, Physics of Fluids. 13 (2001) 1837-1859.

[24] P. Le Tallec, S. Mani, Numerical analysis of a linearised fluid-structure interaction problem, Numerische Mathematik. 87 (2000) 317-354.